Separation Science and Technology
Publication details, including instructions for authors and subscription information:
http://www.informaworld.com/smpp/title~content=t713708471

Synthesis of Zirconium Phosphate, $HZr_2(PO_4)_3$, in Pores of Silica Beads and Some Ion Exchange Separation Properties of the Composite Obtained

Takao Oi[a]; Hiroaki Takahashi[b]; Saki Fukuyama[a]; Kazuo Shirahata[a]; Yong-Hong Zhang[a]
[a] Faculty of Science and Technology, Sophia University, Chiyodaku, Tokyo, Japan [b] Japan Atomic Energy Agency, Tokai-mura, Naka-gun, Ibaraki, Japan

To cite this Article Oi, Takao , Takahashi, Hiroaki , Fukuyama, Saki , Shirahata, Kazuo and Zhang, Yong-Hong(2009) 'Synthesis of Zirconium Phosphate, $HZr_2(PO_4)_3$, in Pores of Silica Beads and Some Ion Exchange Separation Properties of the Composite Obtained', Separation Science and Technology, 44: 15, 3679 — 3697
To link to this Article: DOI: 10.1080/01496390903182099
URL: http://dx.doi.org/10.1080/01496390903182099

Separation Science and Technology, 44: 3679–3697, 2009

ISSN: 0149-6395 print/1520-5754 online
DOI: 10.1080/01496390903182099

Taylor & Francis
Taylor & Francis Group

Synthesis of Zirconium Phosphate, $HZr_2(PO_4)_3$, in Pores of Silica Beads and Some Ion Exchange Separation Properties of the Composite Obtained

Takao Oi,[1] Hiroaki Takahashi,[2] Saki Fukuyama,[1] Kazuo Shirahata,[1] and Yong-Hong Zhang[1]

[1]Faculty of Science and Technology, Sophia University, Chiyodaku, Tokyo, Japan
[2]Japan Atomic Energy Agency, Tokai-mura, Naka-gun, Ibaraki, Japan

Abstract: Zirconium phosphate, $HZr_2(PO_4)_3$ (HZP), was synthesized in inner pores of highly porous silica beads, and the ion exchange properties of HZP-loaded silica beads (HZP-SiO_2) thus obtained were examined. The ion exchange properties of HZP-SiO_2 were basically equivalent to those of HZP in the form of powders. Chromatographic lithium isotope separation was attempted using HZP-SiO_2 as column packing material. The heavier isotope was effectively accumulated in the frontal part of the lithium chromatogram. However, the tailing phenomenon was observed at the rear boundary of the chromatogram, and no effective accumulation of the isotope separation effect was observed in the tail.

Keywords: $HZr_2(PO_4)_3$-loaded silica beads, lithium isotopes, lithium isotope separation, separation factor, zirconium phosphate

Received 26 August 2008; accepted 12 May 2009.
Address correspondence to Takao Oi, Faculty of Science and Technology, Sophia University, 7-1 Kioicho, Chiyodaku, Tokyo 102-8554, Japan. Tel.: +81-3-3238-3359; Fax: +81-3-3238-3361. E-mail: t-ooi@sophia.ac.jp

INTRODUCTION

Lithium has two naturally occurring stable isotopes, ^{6}Li and ^{7}Li, and both are very important nuclides in the nuclear industry. Especially, a large demand for enriched or isolated ^{6}Li is expected in the future since it will be required for the tritium breeder blanket in deuterium-tritium fusion reactors. This necessitates the separation of lithium isotopes. Among the various methods of lithium isotope separation, ion exchange chromatography is certainly a candidate for a large-scale production of enriched lithium isotopes. With commercially available organic ion exchange resins as column packing materials, a value of the single-stage separation factor for the lithium isotopes of up to 1.003 has been observed at room temperature (1). Here, the separation factor, S, is defined as,

$$S = \frac{\text{Amount of } ^{7}\text{Li in solution phase}}{\text{Amount of } ^{6}\text{Li in solution phase}} \times \frac{\text{Amount of } ^{6}\text{Li in resin phase}}{\text{Amount of } ^{7}\text{Li in resin phase}} = (^{7}\text{Li}/^{6}\text{Li})_{\text{solution}}/(^{7}\text{Li}/^{6}\text{Li})_{\text{resin}} \quad (1)$$

where $(^{7}Li/^{6}Li)_{A}$ denotes the ^{7}Li-to-^{6}Li isotopic ratio in phase A. An S value of 1.003 is rather small and materials that show large lithium isotope effects have been sought for the development of the lithium isotope separation process with high performance. It has been reported that some inorganic ion exchangers show larger lithium isotope effects, from several times to over one order of magnitude, than those of organic ion exchangers. They include niobic and tantalic acids (2), antimonic acids (3–5), and titanium(IV)/zirconium(IV) phosphates (6,7).

Rhombohedral zirconium(IV) phosphate, $HZr_2(PO_4)_3$, designated hereafter as HZP, shows cation exchange properties. In our previous papers (8,9), we reported that HZP is lithium-isotopically ^{6}Li specific and shows the lithium isotope effect one order of magnitude larger than those of organic ion exchangers. Unfortunately, HZP we synthesized based on the procedure in the literature (10,11) was in the form of fine powders, designated hereafter as HZP(powder), and could not be used as column packing material for the chromatographic separation of lithium isotopes. It is our objective in this work to synthesize HZP in inner pores of highly porous silica beads and to examine some ion exchange properties of the HZP-loaded silica beads, designated hereafter as HZP-SiO_2, thus obtained. The preliminary results of the chromatographic separation of the lithium isotopes using HZP-SiO_2 as column packing material are also reported.

EXPERIMENTAL

Preparation of $HZr_2(PO_4)_3$-Loaded Silica Beads

Highly porous silica beads with diameters of 40 to 60 μm and the specific surface areas of 3.1 to 3.3 m^2/g used in the present study were supplied by Asahi Kasei.

HZP-SiO_2 was synthesized as follows (10–12): To a flask containing 10 g silica beads was added 35 cm^3 of a ZrO^{2+} solution containing 40.6 mmol Zr, and the mixture was stirred at 70°C for 30 min., and then dried by using a rotary evaporator to penetrate ZrO^{2+} ions into the pores of the silica beads as much as possible. To a flask containing those beads was added 50 cm^3 of an oxalic acid solution containing 65 mmol oxalic acid. The mixture was stirred at 70°C for 30 min. and dried by using the rotary evaporator to obtain ZrO^{2+} and oxalic acid-bearing silica beads. To a beaker containing those silica beads was added 40 cm^3 of a H_2NaPO_4 solution containing 40.2 mmol phosphorus. The mixture was stirred at 70°C for 30 min. and then allowed to stand for 2 weeks at 100°C with occasional stirring after its pH was adjusted to 2.0 with NH_3. The solid, the major constituents of which were expected to be the silica beads, inside the pores of which the precursor of HZP, rhombohedral $NH_4Zr_2(PO_4)_3$, designated hereafter as NZP, had been formed, fragments of broken beads and NZP in the form of powders, was then collected by filtration with a glass filter with the pore size of 16 to 40 μm and washed with 4 dm^3 pure water. The NZP-loaded silica beads, designated hereafter as NZP-SiO_2, were separated from other solid materials with a sieve with the mesh size of 38 μm, dried at 100°C, and heated at 600°C for 1 hour to obtain HZP-SiO_2 by the reaction, $NH_4Zr_2(PO_4)_3 \rightarrow HZr_2(PO_4)_3 + NH_3$. The product thus obtained, HZP-SiO_2, was treated with 2 M HCl at 70°C, washed with pure water, dried at 100°C, and then subjected to various measurements.

Measurements

The powder X-ray diffraction (XRD) patterns were recorded by using a Rigaku RINT2100 V/P X-ray diffractometer with the Cu $K\alpha$ radiation in the 2θ range of 5 to 70 degrees at room temperature. Pore size distributions were measured with a micrometritics Pore Sizer 9320 mercury penetration porosimeter. The zirconium and phosphorus contents in HZP-SiO_2 were determined by ICP-atomic emission spectroscopy (ICP-AES) with a Seiko Instruments SPS7700 ICP-AES spectrometer after HNO_3-HF decomposition of an HZP-SiO_2 aliquot. The scanning

electron microscopy (SEM) was carried out with a Hitachi S-4500 scanning electron microscope. Electron probe microanalysis (EPMA) photograph images were taken with a Shimadzu EPMA-8705 electron probe microanalyzer. Concentrations of Group 1 metal ions in solutions were determined by flame photometry with a Daini Seikosha SAS-727 or a Thermo Electron Corp. SOLAAR M mkII atomic absorption spectrometer and those of other cationic elements by ICP-AES. The concentration of the chloride ion was determined by ion chromatography with a Dionex 2000 ion chromatograph with a HPIC-AS4A anion separation column. The specific surface areas were measured by the Brunauer-Emmett-Teller (BET) method with a Micrometrics Flowsorb II 2300. The lithium isotopic ratio, $^{7}Li/^{6}Li$, of a sample of a batch experiment was determined by the surface ionization technique with a Finnigan Mat 261 mass spectrometer, after the chemical form of the lithium was converted to lithium iodide (1). The lithium isotopic ratio of a sample of a chromatographic experiment was determined with a Thermo Electron Corp. X7-ICP-MS ICP-mass spectrometer after the chemical form of the lithium was converted to lithium nitrate (13).

Ion Exchange Properties

The ion exchange properties of HZP-SiO_2 were examined batchwise in four aspects, i.e., the selectivity for Group 1 metal ions, the lithium ion uptake, the H^+/Li^+ ion exchange rate, and the selectivity for the lithium isotopes.

The selectivity for Group 1 metal ions was investigated by measuring their distribution coefficients, K_d, in $cm^3 \cdot g^{-1}$, defined by the formula,

$$K_d = \frac{\text{Amount of cation in 1 g solid phase}}{\text{Amount of cation in 1 cm}^3\text{solution phase}}. \quad (2)$$

For the measurement of ion selectivity under the basic condition, 0.5 g aliquot of HZP-SiO_2 was placed in 10 cm^3 of NH_3-NH_4Cl buffer solution of pH 9.1 containing 0.5 mM of Li^+, Na^+, K^+, Rb^+, and Cs^+ ions at 25°C for 1 week. The HZP-SiO_2 and the solution were then separated by filtration, and the concentrations of the ions in the solution phase were measured. The amount of an ion taken up into the ion exchanger phase was calculated from the concentration difference in the solution phase before and after the ion exchange equilibrium. Under the acidic condition, the ion selectivity was measured in the similar manner except that the buffer solution used was acetic acid-acetate solution of pH 4.9.

The Li^+ ion uptake was measured by equilibrating 0.2 g aliquot of HZP-SiO_2 with 5 cm^3 of 0.1 M lithium hydroxide solution, 0.1 M lithium acetate solution, or 0.1 M lithium chloride solution at 25°C for 1 week. The Li^+ ion uptake per 1 gram of HZP-SiO_2 was calculated from the concentration difference in the solution before and after the equilibrium. Similar experiments were carried out for 0.1 M lithium acetate solution at 40 and 60°C.

The rate of the H^+/Li^+ ion exchange was examined under acidic and basic conditions at 25°C. The measurement under the basic condition was as follows: 0.2 g aliquot of HZP-SiO_2 was immersed in 5 cm^3 of 0.1 M lithium hydroxide solution, and ion exchange between hydrogen ions in the ion exchanger and lithium ions in the solution commenced immediately. An aliquot of the solution was sampled by filtration with a disk filter when the predetermined reaction time elapsed, and the lithium concentration in the sampled aliquot was measured. The amount of lithium ions taken up was calculated from the concentration difference in the solution phase before the start of the experiment and after the predetermined reaction time elapsed. While the initial solution pH was 13.2, the pH value of the solution phase was 12.2 to 13.2 after the commencement of the H^+/Li^+ ion exchange. Similar measurements were made in the acidic condition using 0.2 g HZP-SiO_2 and 5 cm^3 of 0.1 M lithium acetate solution. The solution pH was initially 7.4 and was 5.5 to 5.7 after the commencement of the H^+/Li^+ ion exchange. The results were compared with those for HZP(powder).

The selectivity for the lithium isotopes was estimated batchwise as S value. 0.2 g aliquot of HZP-SiO_2 was placed in 5 cm^3 of 0.1 M lithium acetate solution, and the solution was maintained at 25°C for 1 week. The ion exchanger was then separated from the solution by filtration, and the lithium isotopic ratio, $^7Li/^6Li$, of the solution phase was measured. From the experimental data in the solution phase, S was actually calculated using the following equation (14),

$$S = [r(1 + r)c_0 - r(1 + r_0)c]/[r_0(1 + r)c_0 - r(1 + r_0)c], \qquad (3)$$

where c_0 and c were the lithium concentrations before and after the equilibrium and r_0 and r were the lithium isotopic ratios ($^7Li/^6Li$) before and after the equilibrium, respectively.

Column Chromatography

Column chromatography using HZP-SiO_2 as column packing material was carried out in the breakthrough, reverse breakthrough, or band

displacement manner under various conditions with a 30 cm × 10 mm ϕ or a 100 cm × 10 mm ϕ glass column. Experiments with the 30 cm-long column were to examine the effects of a few operational factors on the shape of the lithium ion chromatogram. The experiments for lithium isotope fractionation were carried out with the 100 cm-long column.

In a breakthrough experiment, the lithium feed solution was introduced from the bottom of the column at a constant flow rate and the effluent coming out of the top of the column was collected into small fractions with a fraction collector. In a reverse breakthrough experiment, lithium ions adsorbed on the HZP-SiO_2 bed were eluted with an eluent and the effluent was collected into small fractions. In a band experiment, a lithium band of a certain width was first formed in the column, and this band was eluted by an eluent and the effluent from the top of the column was collected. For each fraction of the effluent of an experiment, the lithium concentration was determined, and for selected fractions of an experiment using the 100 cm-long column, the lithium isotopic ratios were measured.

In every experiment, the lithium feed solution was the lithium acetate solution and the eluent was the HCl solution, and the temperature was kept constant during the chromatographic operation by circulating thermostatted water through the water jacket attached to the column. For the experiments with the 100 cm-long column, the S value was evaluated using the chromatographic data by the equation (15),

$$S = 1 + \Sigma f_i |R_i - R_0| / [QR_0(1 - R_0)], \tag{4}$$

where f_i is the amount of the lithium ion in the i-th fraction of the effluent, R_i the atomic fraction of ^{6}Li in the i-th fraction, R_0 that in the feed solution, Q the total ion exchange capacity of the HZP-SiO_2 bed, and the summation is taken over all the fractions where R_i differs from R_0.

RESULTS AND DISCUSSION

Synthesis of NZP-SiO_2 and its Characterization

XRD patterns of silica beads as supplied, NZP powders synthesized outside the pores of silica beads and NZP-SiO_2 are shown in Figs. 1a, 1b, and 1c, respectively, and compared with the XDR pattern of NZP in the literature (JCPDS No. 38–0003). It is evident that NZP was synthesized not only in the pores of the silica beads but also in the solution.

XRD patterns of the silica beads thermally treated at 600°C for 1 hour, and HZP(powder) and HZP-SiO_2 obtained by the thermal treatment of NZP powders and NZP-SiO_2, respectively, are given in

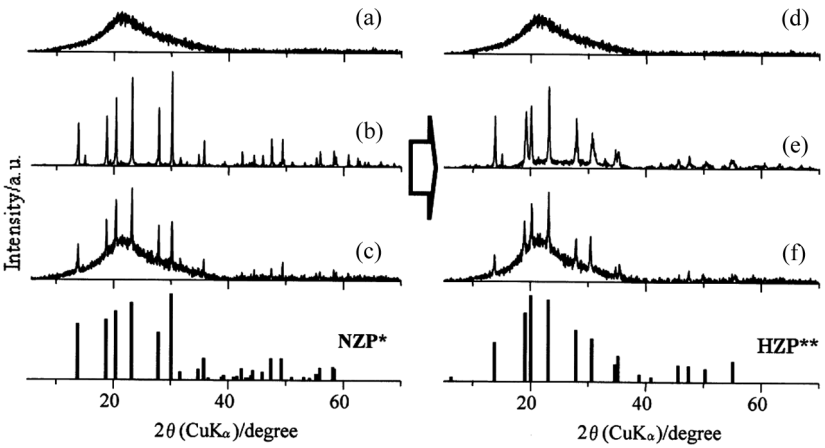

Figure 1. The XRD patterns of (a) silica beads as supplied, (b) NZP powders formed outside the pores of silica beads, (c) NZP-SiO_2, (d) silica beads treated thermally at 600°C for 1 hour, (e) HZP powders obtained from NZP powders, and (f) HZP-SiO_2. *JCPDS No. 38–0003; **JCPDS No. 38–0004.

Figs. 1d, 1e, and 1f, and compared with the XRD pattern of HZP in the literature (JCPDS No. 38–0004). In the XRD pattern of HZP-SiO_2, only the peaks of HZP (and the halo band of SiO_2) were observed. Thus, the crystal phase of HZP-SiO_2 was practically that of rhombohedral HZP alone, with no other crystals in appreciable amounts.

The Zr to P mole ratio of HZP-SiO_2 was 2:2.96 on an average, very close to the stoichiometric value of 2:3, which suggested that the relative amount of impurities (side products) was not substantial, and agreed well with the results of XRD measurements.

The weight percent of HZP in HZP-SiO_2 (degree of HZP loading) was batch-dependent, ranging from 11.3 to 18.3%, with the average of 14.4%. Hereafter, the degree of HZP loading (DL) is specified whenever necessary. The specific surface area of HZP-SiO_2 (DL 18.3%) was $3.66\,m^2/g$, slightly larger than the specific surface area of 3.1 to $3.3\,m^2/g$ of the silica beads as supplied.

An SEM photograph of the surface of a silica bead as supplied is shown in Fig. 2a, and those of a HZP-loaded silica bead in Figs. 2b and 2c. Figure 2c is an enlargement of Fig. 2b. The surface of the HZP-loaded silica bead is very similar to that of the silica bead as supplied and only a few HZP crystals were observed on it as seen in Fig. 2b, which indicated that HZP was scarcely synthesized on the surfaces but in the inner pores of the silica beads. A couple of cube-shaped HZP crystals are observed in the enlarged SEM photograph in Fig. 2c.

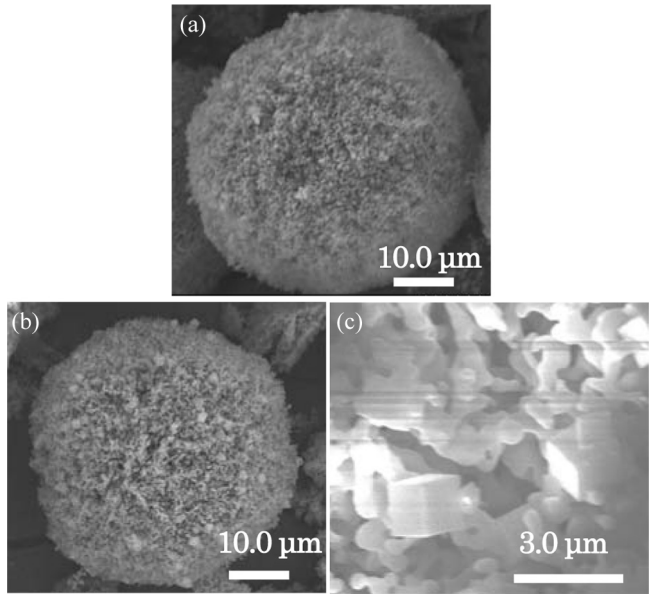

Figure 2. SEM photographs of (a) a silica bead as supplied, (b) a HZP-loaded silica bead, and (c) an enlargement of b.

EPMA images of zirconium and phosphorus on the cross-section of a HZP-loaded silica bead are shown in Figs. 3a and 3b, respectively. As is seen, zirconium and phosphorus distributed nearly uniformly inside the silica bead and their distribution patterns were very similar to each other. This suggested no substantial existence of impurities and agreed well with the results of the XRD analysis and the chemical analysis on the Zr to P ratio in HZP-SiO_2.

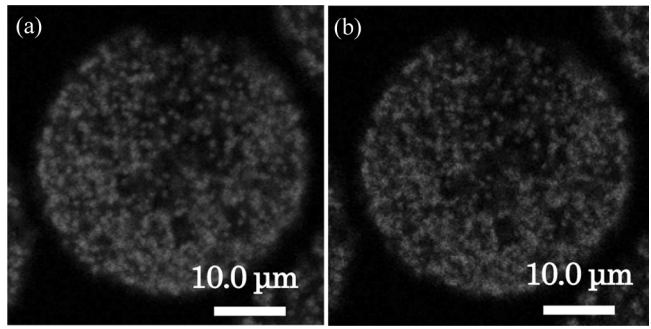

Figure 3. EPMA images of (a) zirconium and (b) phosphorus on the cross-section of a HZP-loaded silica bead.

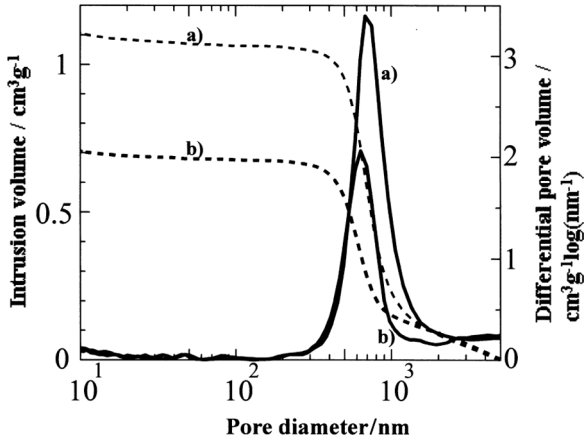

Figure 4. The intrusion volume (left vertical axis) and the differential pore volume (right vertical axis) of (a) silica beads as supplied and (b) HZP-SiO_2 against the pore diameter. – – –: intrusion volume; —: differential pore volume.

Figure 4 depicts the results of mercury penetration porosimetry on the silica beads as supplied and HZP-SiO_2 (DL 18.3%). The plot of the differential pore volume against the pore diameter for the silica beads as supplied had a single sharp peak in the pore diameter range of 10 to 2000 nm, which indicated that the silica beads we used had rather uniform pore volumes. Most of the pore diameters were between 500 to 1000 nm. Upon the formation of HZP in the pores of the silica beads, both the pore diameter and the pore volume decreased, which indicated that part of the pores of the silica beads were occupied by HZP powders. Especially, a comparison of the two differential pore volume distributions revealed that the drastic decrease upon HZP formation occurred in the pore diameter range of 600 to 2000 nm, which indicated that the HZP powders with those sizes were formed in the pores of the silica beads.

A combination of all of the above-mentioned measurements strongly indicated that HZP was synthesized in the pores of the silica beads rather uniformly and scarcely on their surfaces, and that the amount of the side products was inconsiderable.

Ion Exchange Properties

The logarithms of K_d values of Group 1 metal ions on HZP-SiO_2 (DL 13.6%) are plotted in Figs. 5a and 5b, together with those on the HZP(powder). As expected, HZP-SiO_2 and HZP(powder) had a similar

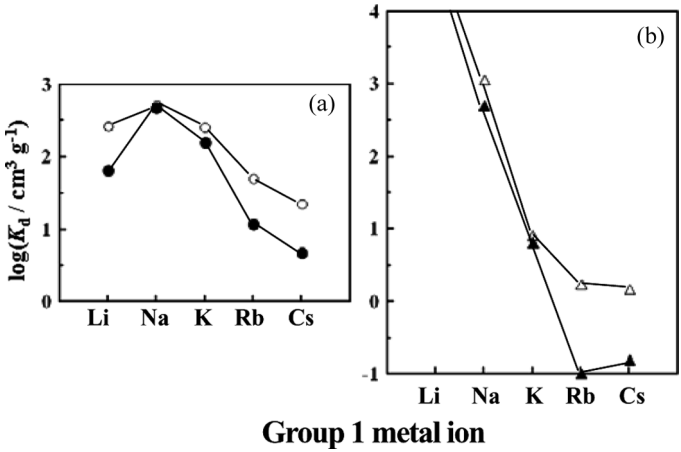

Figure 5. Plots of distribution coefficients (K_d) of Group 1 metal ions (a) on HZP-SiO_2 (●) and HZP(powder) (○) under the acidic condition (pH 4.9), and (b) on HZP-SiO_2 (▲) and HZP(powder) (Δ) under the basic condition (pH 9.1). The logK_d values of the Li^+ ion on HZP-SiO_2 and on HZP(powder) under the basic condition are above 4. Their exact values were not obtained since practically no Li^+ ions were left in the solutions after the ion exchange equilibrium.

selectivity for Group 1 metal ions. In the basic condition, both the ion exchangers showed the very high selectivity towards the lithium ion and little affinity for rubidium and cesium ions. As has been discussed before (9), this indicated that the sizes of the ion exchange sites inside the HZP crystals of HZP-SiO_2 and HZP(powder) were best fitted to the lithium ion and too small for the potassium and larger ions. However, it should be noted that the selectivity for rubidium and cesium ions on HZP-SiO_2 was lower than that on the HZP(powder). This may be due to the fact that the crystal sizes of HZP formed in the pore of the silica beads were larger than those of HZP(powder) and thus the relative number of ion exchange sites, which were located on the surfaces of HZP crystals and were not lithium ion-specific, was smaller in HZP-SiO_2 than in HZP(powder). In the acidic condition (Fig. 5a), the difference in K_d value among Group 1 metal ions was much smaller than in the basic condition, and the highest selectivity was observed for the sodium ion both on HZP-SiO_2 and HZP(powder). This may be related to the nature of HZP as a relatively weak acid.

The lithium ion uptake by HZP-SiO_2 (DL 18.3%) was 2.1, 0.32, and 0.22 mmol/g for lithium hydroxide (the final pH 12.0), lithium acetate (pH 5.5) and lithium chloride (pH 2.5) solutions, respectively, at 25°C. It was thus an increasing function of pH due to the nature of HZP as

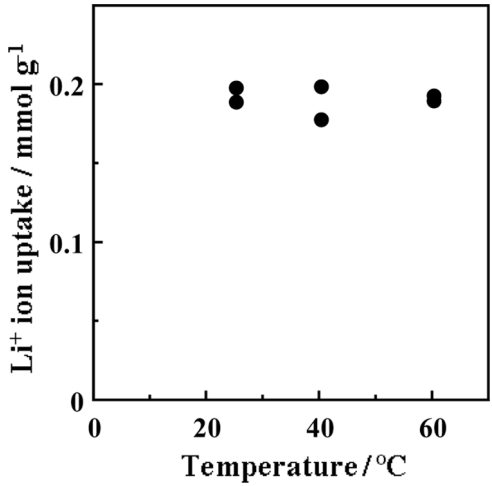

Figure 6. Plot of lithium ion uptake against temperature.

weak acid. The net lithium ion uptake per gram of HZP in HZP-SiO_2 was nearly equal to that of HZP(powder) (9). The lithium ion uptake by HZP-SiO_2 (DL 11.5%) was plotted against the temperature in Fig. 6. It was practically independent of temperature in the range of 25 to 60°C.

The lithium ion uptake by HZP-SiO_2 (DL 11.2%) under the acidic and basic conditions at 25°C is plotted against the ion exchange reaction time in Fig 7, together with that by the HZP(powder). The behavior on HZP-SiO_2 under the acidic condition was very similar to that on the HZP(powder) but with the different absolute value of the lithium uptake. The lithium ion uptake was nearly constant at the reaction times of 3 hours and longer, meaning that the ion exchange equilibrium was attained in about 3 hours at 25°C as in the case of HZP(powder). The behavior on HZP-SiO_2 under the basic condition was quite different both from that under the acidic condition and from that on HZP(powder) under the basic condition. The behavior at the early stage of the lithium ion uptake by HZP-SiO_2 under the basic condition (up to 10 hours) resembled that under the acidic condition, but after that period, the lithium ion uptake started increasing, and seemed to increase gradually even at 172 hours. The lithium ion uptake at the reaction time of 172 hours exceeded the ion exchange capacity of HZP-SiO_2 calculated from the chemical formula of HZP and the degree of the HZP loading. This was ascribable in most part to the decomposition of the skeleton structure of HZP under the basic condition and the consequent revelation of new ion exchange sites: P-O-Zr $\rightarrow$ P-O^- + Zr-O^- as is often the case

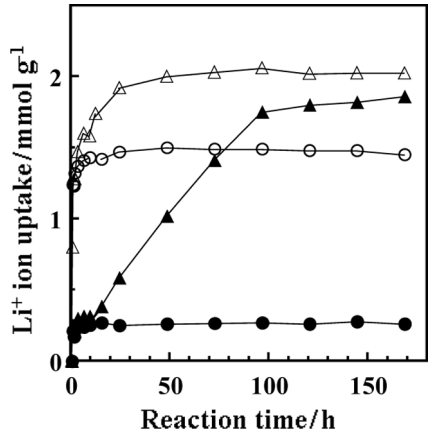

Figure 7. Plots of lithium ion uptake against the reaction time on HZP-SiO_2 under the acidic condition (●) and under the basic condition (▲) and on HZP(powder) under the acidic condition (○) and under the basic condition (Δ).

with zirconium and titanium phosphates (7). A similar phenomenon was observed, albeit much less drastic, for the HZP(powder). The difference in behavior of the lithium ion uptake under the basic condition between HZP-SiO_2 and the HZP(powder) indicated that zirconium phosphate synthesized in the pores of silica beads were less stable than the HZP(powder) formed in the solution.

The *S* value obtained on HZP-SiO_2 (DL 18.3%) batchwise was 1.022 at 25°C, slightly smaller than those we reported for the HZP(powder) in our previous papers (8,9).

Column Chromatography

Experimental conditions of some selected chromatographic experiments using the 30 cm-long column and HZP-SiO_2 (DL 11.5%) as column packing material are summarized in the upper part of Table 1 and the experimental results are shown in Figs. 8 to 10. In Fig. 8 are depicted the chromatograms of two breakthrough experiments, Runs b1 and b2, for which the operating temperature was different, while the other operating parameters were set nearly equal, to examine the temperature effect on the shape of the breakthrough chromatogram. As can be seen in Fig. 8, no drastic difference in the shape of the chromatogram was observed between 40 and 80°C, both the chromatograms having the self-sharpening frontal boundary. This indicated that, in the temperature

Table 1. Experimental conditions and results of selected chromatographic experiments

Run No.	Column	Operating manner[a]	Feed solution	Eluent	Temperature/°C	Flow rate/$cm^3\,hr^{-1}$	S	Figure
b1	30 cm × 10 mmϕ	bt	0.10 M lithium acetate		40	5.8		8 (solid line)
b2		bt	0.11 M lithium acetate		80	5.6		8 (broken line)
rb1		rbt	0.10 M lithium acetate	0.10 M HCl	40	5.8		9, 10 (solid line)
rb2		rbt	0.11 M lithium acetate	0.10 M HCl	80	5.3		9 (broken line)
rb3		rbt	0.10 M lithium acetate	0.10 M HCl	40	13.3		10 (broken line)
b10	100 cm × 10 mmϕ	bt	0.11 M lithium acetate		40	5.1	1.025	11
rb10		rbt	0.11 M lithium acetate	0.10 M HCl	40	5.5	1.025	12
11		b	0.11 M lithium acetate	0.10 M HCl	40	5.8	1.021	13

[a]bt = breakthrough; rbt = reverse breakthrough; b = band.

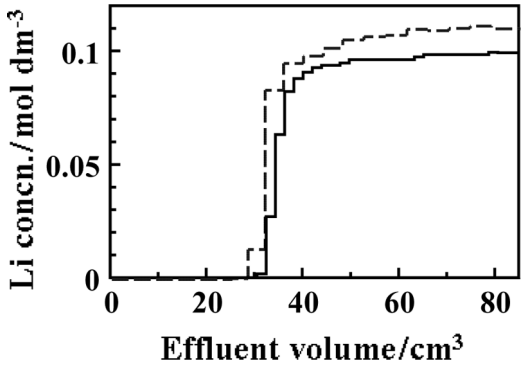

Figure 8. Chromatograms of breakthrough experiments using a 30 cm-long column (run b1,—; run b2,– – –). The experimental conditions are summarized in Table 1.

range of 40 to 80°C, a higher temperature did not improve the H^+/Li^+ ion exchange rate much. We also notice that, even after its rapid increase between the effluent volume of about 30 (the breakthrough point) and 40 cm^3, the lithium ion concentration was still gradually increasing, asymptotically approaching the value in the feed solution in both the runs. This meant that the ion exchange equilibrium was not yet attained even at the effluent volume of 80 cm^3 (Fig. 8), suggesting the existence of the small amount of the ion exchange sites with very slow ion exchange rates.

The effect of the operating temperature on the shape of the reverse breakthrough chromatogram is shown in Fig. 9. As in the case of breakthrough operation, no drastic difference in chromatogram was observed between 40 (Run rb1) and 80°C (Run rb2), with both the runs showing the sharp rear boundary. The tailing phenomenon was observed in both the chromatograms, and the degree of the tailing seemed slightly more substantial at a higher temperature. We also carried out reverse breakthrough experiments at a lower temperature of 25°C, but we could not eliminate the tailing phenomenon.

The effect of the flow rate on the shape of the lithium chromatogram was examined and is shown in Fig. 10 for the reverse breakthrough operation; the result at the flow rate of 5.8 $cm^3\,hr^{-1}$ (Run rb1) is compared with the one at 3.3 $cm^3\,hr^{-1}$ (Run rb3). As is seen, a slower flow rate seemed to result in a slightly sharper rear boundary, but the change was not substantial. No substantial difference in the degree of the tailing was observed, either.

Thus, experiments with the 30 cm long column showed that, within the temperature range of 40 to 80°C and within the flow rate range of

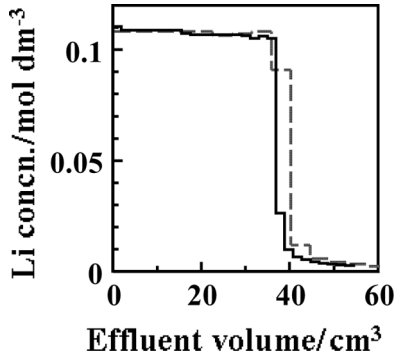

Figure 9. Chromatograms of reverse breakthrough experiments using a 30 cm-long column (run rb1,—; run rb2,– – –). The experimental conditions are summarized in Table 1.

5.8 to 13.3 $cm^3\,hr^{-1}$, the lithium chromatogram did not change much, having sharp frontal and rear boundaries with a tail.

The conditions and results of the experiments using the 100 cm-long column are summarized in lower part of Table 1. The lithium chromatograms and the lithium isotope fractionation profiles of the experiments are depicted in Figs. 11 to 13. In each figure, the Li^+ ion concentration is shown by the solid line (the left vertical axis) and the lithium isotopic data by the filled circles (the right vertical axis). The isotopic datum of a fraction of the effluent is given as the $^7Li/^6Li$ isotopic ratio of that fraction divided by that of the feed solution, $(^7Li/^6Li)_i/(^7Li/^6Li)_{orig}$, often called the "local enrichment factor."

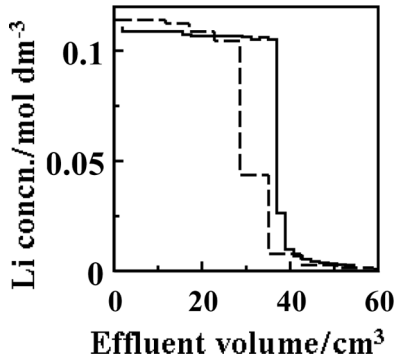

Figure 10. Chromatograms of reverse breakthrough experiments using a 30 cm-long column (run rb1,—; run rb3,– – –). The experimental conditions are summarized in Table 1.

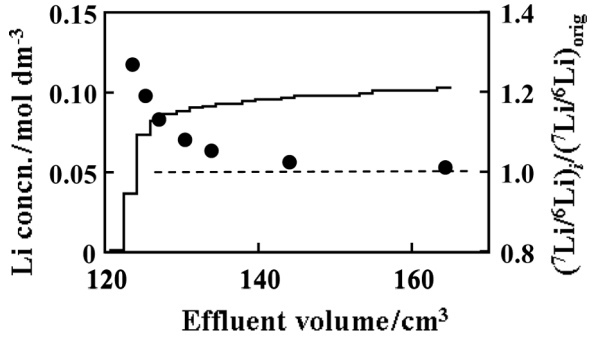

Figure 11. The chromatogram (—) and the lithium isotope fractionation profile (•) of the breakthrough experiment (Run b10) using a 100 cm-long column.

In Fig. 11 is depicted the result of the breakthrough experiment (Run b10). It is seen that $(^7Li/^6Li)_i/(^7Li/^6Li)_{orig}$ was a monotonously decreasing function of the effluent volume and asymptotically approached the original value with increasing effluent volume. Thus, the heavier isotope of lithium was enriched in the frontal part of the breakthrough chromatogram, meaning that the same isotope was preferentially fractionated in the solution phase as was usually the case with the ion exchange system (1,3,5). This trend in the lithium isotope fractionation agreed with that found in the batch experiment. The S value was 1.025.

The results of the reverse breakthrough experiment (Run rb10) are shown in Fig. 12. Except for the tailing part, $(^7Li/^6Li)_i/(^7Li/^6Li)_{orig}$ was a monotonously decreasing function of the effluent volume, showing the preferential adsorption of the lighter isotope into the exchanger phase and the expected chromatographic accumulation of the single-stage

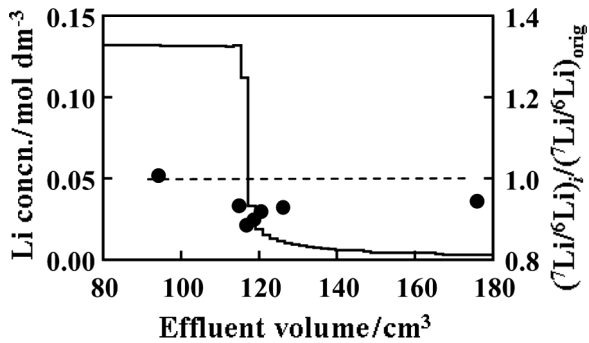

Figure 12. The chromatogram (—) and the lithium isotope fractionation profile (•) of the reverse breakthrough experiment (Run rb10) using a 100 cm-long column.

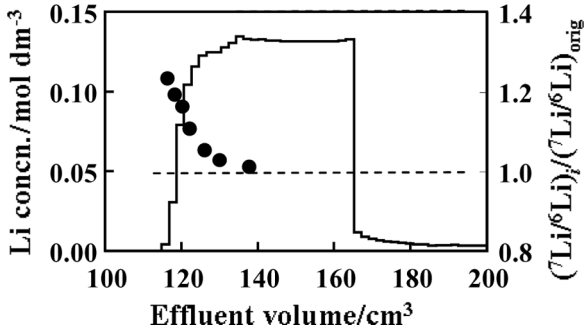

Figure 13. The chromatogram (—) and the lithium isotope fractionation profile (●) of the band experiment (Run 11) using a 100 cm-long column.

isotope separation. However, in the tail region, isotope accumulation was not accomplished well. Figure 12 thus clearly shows the tailing phenomenon should be avoided for the effective accumulation of the isotopes in the chromatographic isotope separation processes. The S value was 1.025, the same as the one obtained in the breakthrough experiment (Run b10).

The results of the band experiment (Run 11) are depicted in Fig. 13. Except for the tail part, the shape of the chromatogram was nearly of band displacement type. The isotopic ratio measurements were made only for the frontal half of the band, since the effective accumulation of the lithium isotopes was not expected in the rear part due to the tailing phenomenon. As in the case of the breakthrough experiment, the accumulation of the heavier isotope was observed, and $(^7Li/^6Li)_i/(^7Li/^6Li)_{orig}$ was a monotonously decreasing function of effluent volume. The S value was 1.021, slightly smaller than those of the breakthrough and reverse breakthrough experiments, probably due to the slight mixing of the frontal enriching part of the heavier isotope and the rear depleting part of the same isotope.

The S values obtained chromatographically were slightly larger than those obtained in the batch experiment (1.025 at 40°C vs. 1.022 at 25°C). The former was more reliable than the latter, since the isotope separation effect in a single-stage was accumulated in the chromatographic experiments.

CONCLUSION

In the present study, we tried to synthesize rhombohedral zirconium phosphate, $HZr_2(PO_4)_3$, in the inner pores of porous silica beads and

examined ion exchange properties of the $HZr_2(PO_4)_3$-SiO_2 composite ion exchanger thus obtained. To summarize, we make the following statements:

1. Zirconium phosphate (HZP) was successfully synthesized in the pores of the silica beads with only a few HZP crystals observed on the surfaces of the beads. The degree of HZP loading (w/w%) was batch-dependent, ranging from 11.2 to 18.3%.
2. The ion exchange property of the HZP-loaded silica beads (HZP-SiO_2) examined by the batch experiments was basically equivalent to that of HZP in the form of fine powders.
3. Column chromatography was carried out to examine the performance of HZP-SiO_2 as the column packing material for the chromatographic lithium isotope separation. The self-sharpening frontal boundary of the lithium chromatogram was formed and the steady isotope accumulation was observed in the frontal part of the chromatogram where the heavier isotope of lithium was enriched. The tailing phenomenon was observed in the rear part of the chromatogram, and, in the tail, the single-stage isotope separation effect was not accumulated effectively. The elimination of tailing seemed very important to establish the chromatographic lithium isotope separation process with high performance using HZP-SiO_2.

ACKNOWLEDGEMENTS

We would like to acknowledge Professor Y. Fujii, Tokyo Institute of technology (Titech) for offering the use of mass spectrometers and Dr. M. Nomura, Titech, for his assistance in the measurement of lithium isotopic ratios.

REFERENCES

1. Oi, T.; Kawada, K.; Hosoe, M.; Kakihana, H. (1991) Fractionation of lithium isotopes in cation-exchange chromatography. *Sep. Sci. Technol.*, *26*: 1353; and references cited therein.
2. Inoue, Y.; Kanzaki, Y.; Abe, M. (1996) Isotopic separation of lithium using inorganic ion exchangers. *J. Nucl. Sci. Technol.*, *33*: 671.
3. Oi, T.; Shimizu, K.; Tayama, S.; Matsuno, Y.; Hosoe, M. (1999) Cubic antimonic acid as column-packing material for chromatographic lithium isotope separation. *Sep. Sci. Technol.*, *34*: 805.
4. Oi, T.; Endoh, M.; Naromoto, M.; Hosoe, M. (1999) Ion and lithium isotope selectivity of monoclinic antimonic acid. *J. Mater. Sci.*, *35*: 509.

5. Oi, T.; Takahashi, S. (2005) Chromatographic lithium isotope separation using cubic antimonic acid as column-packing material. *Sep. Sci. Technol.*, *40*: 1001.
6. Takahashi, H.; Oi, T.; Hosoe, M. (2002) Characterization of semicrystalline titanium(IV) phosphates and their selectivity of cations and lithium isotopes. *J. Mater. Chem.*, *12*: 2513.
7. Takahashi, H.; Zhang, Y.-H.; Miyajima, T.; Oi, T. (2006) Ion exchange properties and selectivity of lithium isotopes on ion exchangers in the hydrogen form prepared from $LiTi_xZr_{2-x}(PO_4)_3$ ($0 \leq x \leq 2$). *J. Mater. Chem.*, *16*: 1462.
8. Oi, T.; Uchiyama, Y.; Hosoe, M.; Itoh, K. (1999) Alkali metal ion and lithium isotope selectivity of $HZr_2(PO_4)_3$. *J. Nucl. Sci. Technol.*, *36*: 1064.
9. Kikuchi, R.; Takahashi, H.; Oi, T.; Hosoe, M. (2003) Selectivity of metal cations and lithium isotopes on ion exchangers prepared by thermal treatment of $NH_4Zr_2(PO_4)_3$. *J. Mater. Sci.*, *38*: 515.
10. Daiichi Kigenso Chem. Ind., Co., Ltd., (1994) Japan Patent, 6–53566, 25 [in Japanese].
11. Daiichi Kigenso Chem. Ind., Co., Ltd., (1995) Japan Patent, 7–115851, 65 [in Japanese].
12. Takahashi, H. (2005) Adsorptive removal of silver from simulated spent fuel solution. Reports of Institute of Research and Innovation, 25: 5 [in Japanese].
13. Otake, K.; Kaneshiki, T.; Suzuki, T.; Nomura, M.; Fujii, Y. (2007) Lithium isotope separation by crown ether resins with different cavity size. *Proc. Spring Meeting Atomic Energy Soc. Jpn.*, *593* [in Japanese].
14. Ooi, K.; Feng, Q.; Kanoh, H.; Hirotsu, T.; Oi, T. (1995) Lithium isotope fractionation on inorganic ion exchangers with different ion-sieve properties. *Sep. Sci. Technol.*, *30*: 3761.
15. Kakihana, H.; Kanzaki, T. (1969) A simplified and generalized method for analyzing chromatographic isotope separation data. Bull. *Tokyo Inst. Technol.*, *90*: 77.